Journal of Alloys and Compounds, 203 (1994) 221–227
JALCOM 873

Structural stability and thermodynamic properties of Zr–N alloys

Toru Ogawa
Japan Atomic Energy Research Institute, Tokai-mura, Naka-gun, Ibaraki-ken 319-11 (Japan)

(Received April 19, 1993; in final form July 1, 1993)

Abstract

The phase diagram and thermodynamic properties of Zr–N alloys were modelled by presupposing the existence of the mononitrides with their metal sublattices having f.c.c., h.c.p. and b.c.c. structures. Each phase in the system was assumed to be composed of a filled metal sublattice and a partially filled non-metal sublattice. The lattice stability parameters of the h.c.p. and b.c.c. mononitrides were estimated from the salient features of the phase diagram. Without any particular effort to fit the model parameters to the existing experimental data, the thermodynamic properties of the alloys are predicted with reasonable accuracy. Crystallographic aspects related to the possible ω-phase-like lattice distortion of the b.c.c.-Zr–N alloys are also discussed.

1. Introduction

When we deal with a phase diagram, we see the minimum free-energy (G) surface or an approximation of it. However, if we could put our heads a little above the minimum G surface, we should see varieties of structural possibilities. The structural energy differences among alternative structures have been defined in terms of the lattice stability energies for pure metals [1, 2] and quantum mechanical explanations of the origin of the structural stability among alternative atomic arrangements have been given for both pure metals and intermetallic compounds [2–4]. Generally the structural energy differences are small fractions of the cohesive energies of metals and alloys.

That there are a range of structural alternatives competing with each other is implicit in the thermodynamic analyses of phase diagrams. In some cases it is even useful to presuppose structural alternatives which are not only absent in the phase diagram but also might not be attained in the laboratory. Those structures are hypothetical in the sense that we would not have them, but real in the sense that they determine the constitution of the alloy systems. The Zr–N binary, for which the thermodynamic properties and the phase diagram have yet to be better defined, is one such system.

2. Analysis

2.1. Formalism

In the absence of detailed information on transition metal–nitrogen alloys, the Engel–Brewer theory [5] gives useful guidance. The theory correlates the long-range order of the metal lattice with the number of s and p valence electrons per metal atom. With increasing s and p electrons, b.c.c., h.c.p. and f.c.c. structures are stabilized in that order. Addition of N atoms to the metal lattice increases the p electron concentration to stabilize the h.c.p. *vs.* the b.c.c. structure and then the f.c.c. *vs.* the h.c.p. structure. (This does not necessarily mean that electrons are transferred from N to the metal. Complex non-metal–p and metal–d interactions in the transition metal carbides and nitrides have been analysed via band structure calculations by Schwartz and coworkers [6, 7]).

Figure 1 shows the Zr–N alloy phase diagram [8]. Below the solidus there are two series of solid solutions, α-Zr(N) and β-Zr(N) with h.c.p. and b.c.c. structures respectively, and a non-stoichiometric compound ZrN_{1-x} with an NaCl-type structure. The general behaviour of the system follows the trend predicted by the Engel–Brewer theory. The α(h.c.p.)–β(b.c.c.) transition temperature is raised with increasing nitrogen concentration, while further addition of nitrogen leads to f.c.c.-ZrN_{1-x}.

For each phase Ψ in the system the free energy of formation, $\Delta G_f(\Psi)$, can be expressed by the sublattice formalism [9–11].

$$\Delta G_f(\Psi) = Y_V \Delta G_f^\circ(\Psi\text{-Zr}) + Y_N \Delta G_f^\circ(\Psi\text{-ZrN}) - T\Delta S_{ideal} + \Delta G^{EX}$$

Here the phase Ψ is regarded as a series of solutions of pure Ψ-Zr and the stoichiometric mononitride, the

0925-8388/94/$07.00
SSDI 0925-8388(93)00873-W

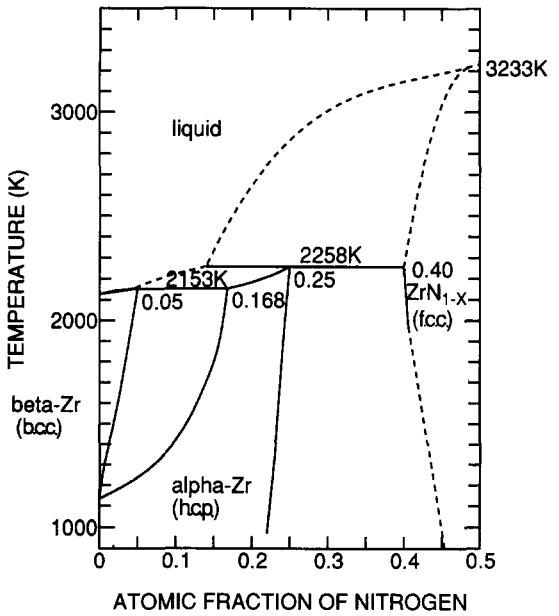

Fig. 1. Phase diagram of the system Zr–N [6].

latter having the same structure of metal sublattice as Ψ-Zr. This is equivalent to regarding the structure of Ψ as consisting of a filled metal sublattice and a partly filled non-metal sublattice. Y_N and Y_V are the fractions of nitrogen atoms and vacancies in the non-metal sublattice respectively, with $Y_N + Y_V = 1$. The atomic fraction of nitrogen is $X_N = Y_N/(1+Y_N)$. The ideal entropy of mixing, ΔS_{ideal}, is given by

$$\Delta S_{ideal} = -R(Y_N \ln Y_N + Y_V \ln Y_V)$$

The excess free energy of mixing, ΔG^{EX}, is expressed by the Redlich–Kister equation [12]

$$\Delta G^{EX} = \sum_i Y_V Y_N \Omega_i (Y_V - Y_N)^{i-1}$$

where the Ω_i are polynomial coefficients. Each polynomial coefficient could be a function of temperature.

In the above formulation we presuppose the existence of the mononitrides with their metal sublattices having b.c.c. and h.c.p. structures, which do not appear in the phase diagram. The crystallographic aspects of such nitrides are discussed in a later section.

There may be alternative approaches, *e.g.* finding the model parameters from least-squares fitting of the phase diagram and existing thermodynamic data [13–15]. Such an approach, however, is difficult for this particular alloys system, where even the liquidus is not well defined. The following sections show the usefulness of the present method in predicting the thermodynamic properties of the Zr–N system.

2.2. *Free energies of formation*

In the first step we shall neglect ΔG^{EX}. In the following discussion the hypothetical melting point (T_m) of an alternative structure Ψ is introduced:

$$T_m(\Psi) = \frac{\Delta H_m(\Psi \rightarrow L)}{\Delta S_m(\Psi \rightarrow L)}$$

$$\Delta H_m(\Psi \longrightarrow L) = \sum_i^k \Delta H(\Psi \longrightarrow \Psi_i) + \Delta H_m(\Psi_k \longrightarrow L)$$

$$\Delta S_m(\Psi \longrightarrow L) = \sum_i^k \Delta S(\Psi \longrightarrow \Psi_i) + \Delta S_m(\Psi_k \longrightarrow L)$$

Here ΔH and ΔS are the enthalpy and entropy of transition respectively and the Ψ_i ($i = 1,2,\ldots,k$) indicate the alternative structures with the same composition as Ψ. L denotes the liquid.

In Fig. 2 salient features of the Zr–N phase diagram are shown. With the above formulation this diagram is delineated as follows.

(1) Boundaries between the h.c.p. and f.c.c. phases are almost vertical lines in the diagram. Conversely, their extensions hardly intersect the ordinates at $Y_N = 0$ and 1. This is interpreted as showing the following inequalities *at all temperatures below* T_m:

$$\Delta G_f^\circ(\text{h.c.p.-Zr}) < \Delta G_f^\circ(\text{f.c.c.-Zr})$$

$$\Delta G_f^\circ(\text{h.c.p.-ZrN}) > \Delta G_f^\circ(\text{f.c.c.-ZrN})$$

Similarly we can assume the inequality

$$\Delta G_f^\circ(\text{b.c.c.-ZrN}) > \Delta G_f^\circ(\text{h.c.p.-ZrN})$$

since the boundaries tend to be vertical with increasing Y_N. Without a significant loss in accuracy we may assume the following relation independent of the temperature:

$$\Delta G_f^\circ(\Psi_i\text{-ZrN}) - \Delta G_f^\circ(\Psi\text{-ZrN}) = \Delta H(\Psi\text{-ZrN} \longrightarrow \Psi_i\text{-ZrN})$$

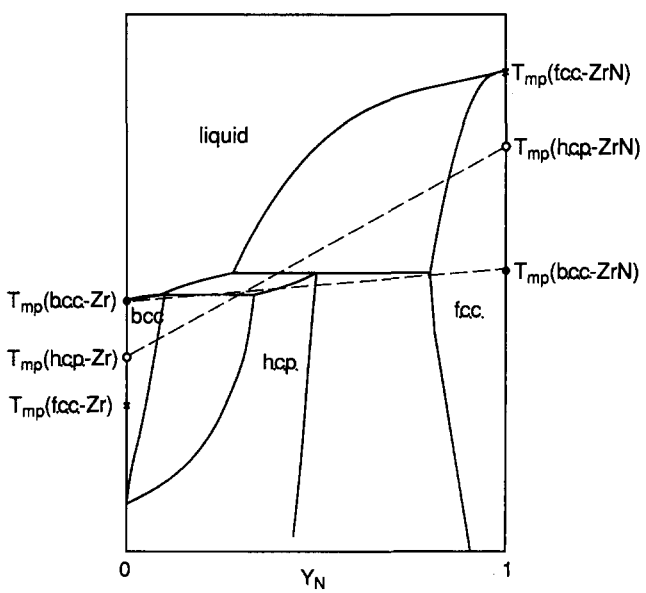

Fig. 2. Schematic phase diagram of the system Zr–N and melting points of Zr and ZrN with various structures.

(2) T_m of pure h.c.p.-Zr lies on the extensions of the liquidus and solidus of the h.c.p. phase to $Y_N = 0$. Thus we would find T_m(h.c.p.-ZrN) on the extensions to $Y_N = 1$. Similarly we would find T_m(b.c.c.-ZrN) at $Y_N = 1$.

(3) The width of the liquid–solid two-phase region increases in the order b.c.c. → h.c.p. → f.c.c. As long as the liquid is ideal or nearly regular, the width of the two-phase region is larger for the solid solution phase with the minimum of its ΔG_f lying towards a larger Y_N. Therefore we would find

$$-\Delta G_f^\circ(\text{b.c.c.-ZrN}) < -\Delta G_f^\circ(\text{h.c.p.-ZrN}) < -\Delta G_f^\circ(\text{f.c.c.-ZrN})$$

This order is not only supported by the observations (1) and (2) but also agrees with the trends predicted by the Engel–Brewer theory.

(4) The width of the liquid–b.c.c. two-phase region is very narrow. This suggests that the absolute values of interaction parameters of the liquid and b.c.c. phases are small. Considering our position in (3) also, we may assume that the liquid phase is ideal.

On the basis of these observations, particularly (1) and (2), we can first estimate ΔG_f°(b.c.c.-ZrN) and ΔG_f°(h.c.p.-ZrN) from ΔG_f°(f.c.c.-ZrN). ΔG_f°(f.c.c.-ZrN) has been derived from thermal data of Alcock *et al.* [16]. ΔG_f°(f.c.c.-Zr) obtained by Kaufman and Bernstein [1] and the enthalpy of fusion (ΔH_m) of f.c.c.-ZrN estimated by Alcock *et al.* [16] are adopted. The free energies of formation of the components thus derived are listed in Table 1.

The degree of arbitrariness in each extension of solidus and liquidus to $Y_N = 1$ can be compensated by a suitable choice of the coefficients Ω_i.

2.3. *Excess free-energy terms*

The next step is to find a set of polynomial coefficients Ω_i to define ΔG^{EX}. In the estimation almost all we need are the approximate positions of the two peritectic reactions (1) h.c.p. → f.c.c. + liquid and (2) b.c.c. → f.c.c. + liquid. The procedure is as follows.

TABLE 1. Free energies of formation (reference state is α (h.c.p.)-Zr)

Species	ΔG_f°(J mol^{-1})
H.c.p.-Zr	0
B.c.c.-Zr	$3940 - 3.475T$
F.c.c.-Zr	3350
Liq.-Zr	$24870 - 13.315T$
H.c.p.-ZrN	$-357443 + 93.789T$
B.c.c.-ZrN	$-347160 + 93.789T$
F.c.c.-ZrN	$-367355 + 93.789T$
Liq.-ZrN	$-300411 + 73.222T$

TABLE 2. Redlich–Kister parameters for the h.c.p., b.c.c. and f.c.c. phases

Phase	Ω
H.c.p.	$-25600 + 6.23T$
B.c.c.	$-7712 + 4.49T$
F.c.c.	$\Omega_1 = 0$, $\Omega_2 = 40000$

(1) As stated above, we assume $\Omega_{liquid} = 0$.

(2) Find Ω_{fcc} which gives the first peritectic reaction.

(3) Find Ω_{hcp} which gives the first peritectic reaction and also satisfies the h.c.p.–f.c.c. equilibria at lower temperatures.

(3) Find Ω_{bcc} which gives the second peritectic reaction (Fig. 2) and also satisfies the b.c.c.–h.c.p. equilibria at lower temperatures. Besides, Ω_{bcc} should not differ significantly from zero (point (4) in Section 2.2).

Considering the possible experimental errors, reproducing the experimental boundaries within ± 20 K and ± 2 at.% would be satisfactory. The resulting parameters are listed in Table 2. The f.c.c. phase has to be assumed subregular to reproduce the equilibrium compositions in the first peritectic reaction. The b.c.c. phase is regular with a Ω_{bcc} value of only ± 2 kJ mol^{-1}, which changes moderately with temperature.

The equilibria were calculated with the free-energy minimizer CHEMSAGE [17].

3. Results and discussion

3.1. *Phase diagram and partial pressures*

The calculated phase diagram is shown in Fig. 3 and agrees with the assessed diagram (Fig. 1) within experimental error.

The calculated partial pressure of N_2, $p(N_2)$, as a function of composition within the homogeneity range of the nitride is shown in Fig. 4. The experimental partial pressures over ZrN in the literature [18–20] show significant scatter. This scatter is considered to be largely due to the wide homogeneity range of the nitride and the preferential loss of nitrogen from the sample surface: one cannot be sure of the exact composition. Hoch *et al.* [18] have measured the weight loss of the nitride in a Knudsen effusion cell, where most of the weight reduction could be ascribed to the evaporative loss of nitrogen. It is almost impossible to relate $p(N_2)$ to the nitride composition in this type of measurement. Only Khromov and Svistunov [19] have measured $p(N_2)$ over ZrN as a function of the initial bulk composition by a Knudsen cell effusion and mass spectrometric analysis. The calculated $p(N_2)$ agrees well with their data (solid and open circles) within the homogeneity range.

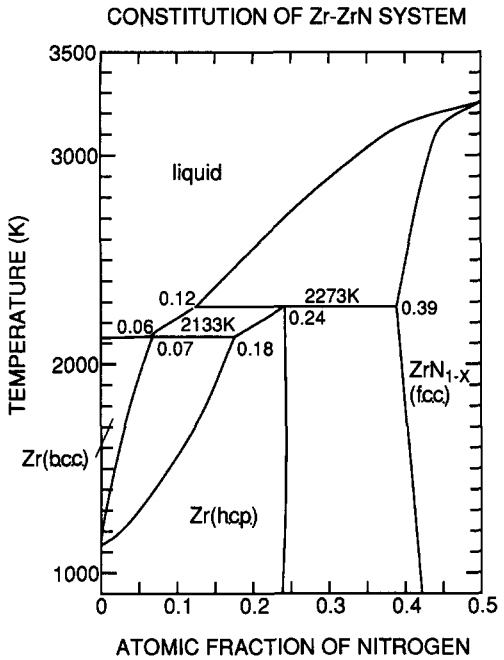

Fig. 3. Calculated phase diagram of the system Zr–N.

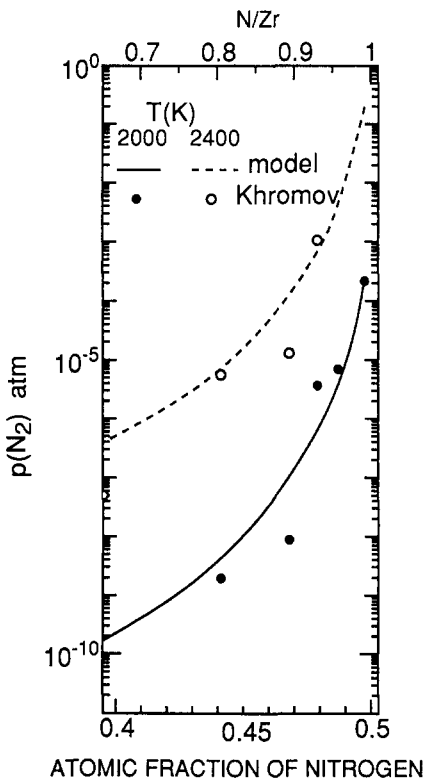

Fig. 4. Calculated (solid curve) and experimental (circles) [17] nitrogen partial pressures in the homogeneity range of ZrN.

The nitrogen-saturated Zr solid solution should eventually precipitate from the nitride as a result of preferential vaporization loss of nitrogen. Values of $p(N_2)$ in the Zr+ZrN two-phase region are shown in Fig. 5. The calculated $p(N_2)$ (solid curve) is higher by a factor

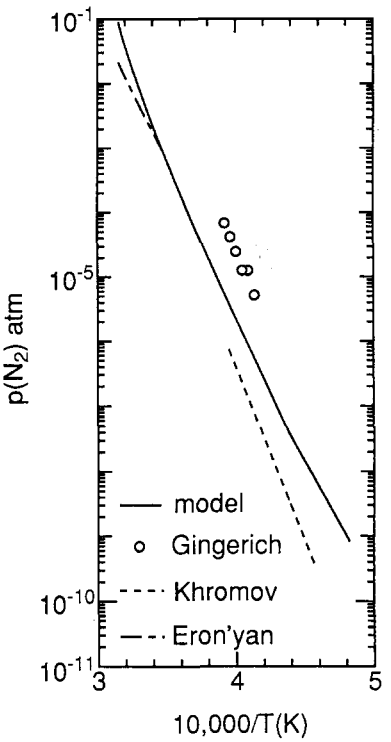

Fig. 5. Calculated (solid curve) and experimental [17–19] nitrogen partial pressures in the two-phase region of h.c.p.-Zr and ZrN_{1-x}.

than the experimental results (dashed line) over a Zr+ZrN mixture obtained by Khromov and Svistunov [19]. Gingerich [20] has applied a Knudsen cell effusion and mass spectrometric analysis to a commercially obtained sample of approximate overall composition $Zr_{0.64}N_{0.31}O_{0.05}$, which would be in the Zr+ZrN two-phase region. He obtained $p(N_2)$ (open circles) higher than the model prediction. However, particles in commercially obtained ZrN powder often show a large degree of inhomogeneity when they contain a significant amount of oxygen. Eron'yan *et al.* [21] have measured the temperature at which the liquid metal appears on the surface of *in situ* prepared ZrN sheet under a given nitrogen pressure. The measurements gave a $p(N_2)$ over the Zr+ZrN mixture (chain line) which agrees with the model prediction at about 3000 K, but the agreement deteriorates with increasing temperature.

The above comparisons indicate that the accuracy of the model prediction is comparable with that of careful measurements. The present model is considered to give a reasonable description of the vaporization behaviour of ZrN.

Figure 6 shows the Zr activity $a(Zr)$ and $p(N_2)$ in the b.c.c., h.c.p. and f.c.c. phases at 2000 K. In each phase the activity coefficient of Zr is greater than or equal to unity at the lower phase boundary but decreases with increasing nitrogen constant. In other words, Zr is stabilized in each phase with increasing nitrogen content. At the same time $p(N_2)$ increases progressively

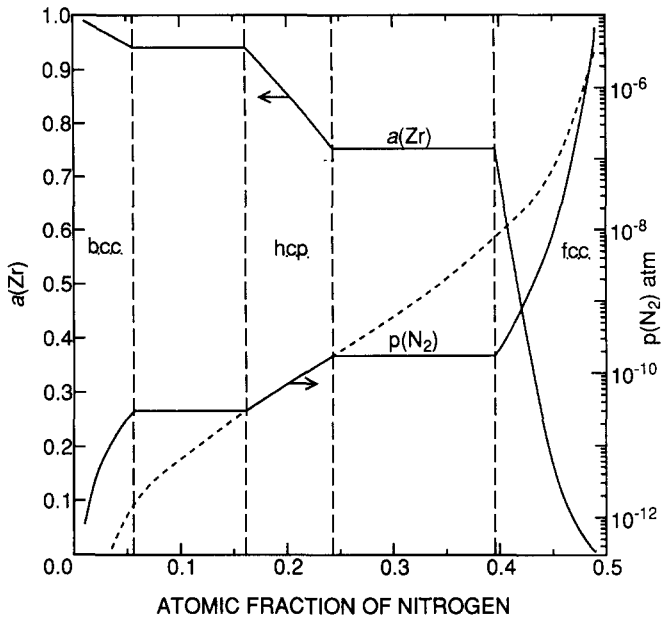

Fig. 6. Component activities at 2000 K as a function of nitrogen content. a(Zr) refers to pure b.c.c.-Zr. The dashed curve gives $p(N_2)$ over the h.c.p.-Zr phase in the regions where this phase is unstable.

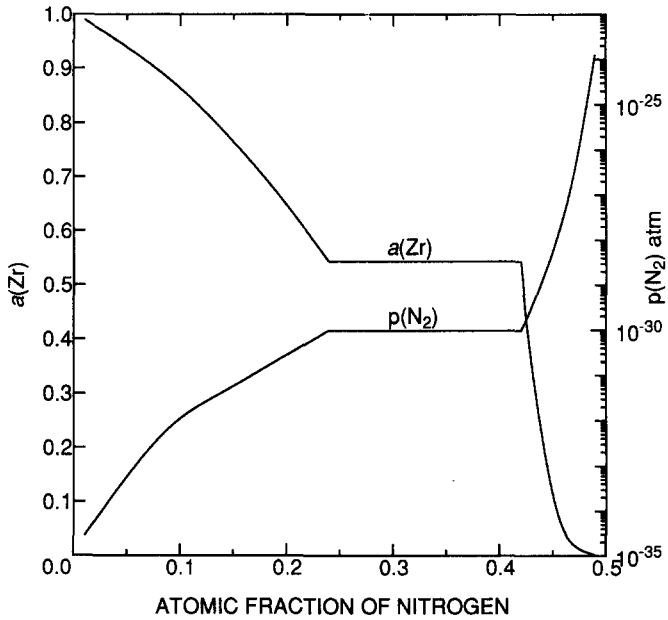

Fig. 7. Component activities at 973 K as a function of nitrogen content. a(Zr) refers to pure h.c.p.-Zr.

with increasing nitrogen content. Eventually the given phase is overtaken by the other phase which better accommodates nitrogen. In the figure $p(N_2)$ in the h.c.p. phase is shown by a dashed curve in the regions where this phase is unstable. As expected, nitrogen is stabilized in the following order: b.c.c. < h.c.p. < f.c.c.

The zirconium activity a(Zr) and $p(N_2)$ at a low temperature of 973 K are plotted in Fig. 7. Itoh *et al.* [22] have studied the reactions of U–Zr alloys with nitrogen. At 973 K they found that α-Zr (h.c.p.-Zr) containing about 20 at.% N ($X_N \approx 0.2$) is in equilibrium with an alloy of approximate composition $U_{0.9}Zr_{0.1}$. The value of a(Zr) is about 0.65 in the latter alloy [23], which agrees with the predicted value of a(Zr) in the alloy of approximate composition α-$Zr_{0.8}N_{0.2}$. The equilibria in the ternary system U–Zr–N will be discussed in more detail elsewhere [24].

3.2. Crystallographic aspects

The assumption that the metal sublattice is filled and the non-metal sublattice is a mixture of nitrogen atoms and vacancies agrees with the lattice parameter and density measurements on f.c.c.-ZrN_{1-x} [25].

There are nitrides and carbides that have a metal sublattice with the h.c.p. structure [26]. δ'-NbN has the anti-NiAs structure, in which the Nb atoms occupy the As positions and the N atoms the Ni positions. Each N atom is surrounded by six Nb atoms in an octahedral coordination. With the other transition metals, anti-NiAs structural derivatives such as L_3' (Fe_2N type) are more common [26]. Howe [27] confirmed experimentally that the N atoms in α-Zr occupy the octahedral sites. Therefore we may safely regard α-Zr(N) as a solution of h.c.p.-Zr and h.c.p.-ZrN.

On the contrary, it is hard to imagine a mononitride with the b.c.c. metal sublattice, since the interstitial cavities in the b.c.c. metals are too small to neatly accommodate the N atoms. However, there is a modification of tantalum nitride, ϵ-TaN [28, 29], whose structure appears to be related to the b.c.c. structure as discussed below.

ϵ-TaN has one Ta atom at the point position 1(a), two Ta atoms at 2(d) and three N atoms at 3(f) in space group *P6/mmm*. The atomic coordinates are:

		x	y	z
Ta(1)	1(a)	0	0	0
Ta(2)	2(d)	$\frac{1}{3}$	$\frac{2}{3}$	$\frac{1}{2}$
N	3(f)	0.393	0	0

The Ta(1) atoms form a centred hexagon and the Ta(2) atoms an uncentred hexagon. The metal sublattice thus consists of alternating layers of two types of hexagons, which reminds us of the hexagonal lattice of the metastable ω phase of zirconium-based alloyds [30]. The ω phase is oriented with respect to the original b.c.c. phase (Fig. 8): $\langle 0001\rangle_{hex} \| \langle 111\rangle_{bcc}$ and $\langle 2\bar{1}\bar{1}0\rangle_{hex} \| \langle \bar{1}01\rangle_{bcc}$. The original atomic positions in the b.c.c. cell viewed in the hexagonal cell are (0, 0, 0), $\pm(\frac{2}{3}, \frac{1}{3}, \frac{2}{3})$; the atomic positions in the ω phase are (0, 0, 0), $\pm(\frac{2}{3}, \frac{1}{3}, \sim\frac{1}{2})$. The atomic positions in the ω phase agree with those of the metal atoms in ϵ-TaN. The lattice parameters of the ω phase are thus related to that of the original b.c.c. cell:

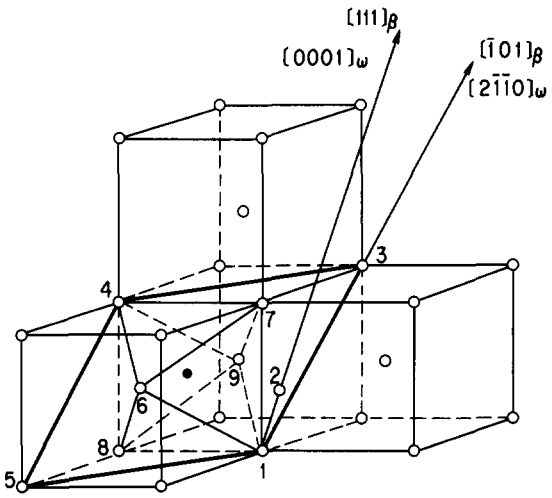

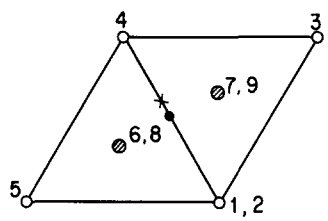

Position	Coordinate in ω lattice			
1, 3–5	0	0	0	
6, 8	$\frac{1}{2}$	$\frac{2}{3}$	$\pm\frac{1}{2}$	
7, 9	$\frac{2}{3}$	$\frac{1}{3}$	$\pm\frac{1}{2}$	
●	$\frac{1}{2}$	0	0	Centre of octahedron[a]
×	–	0	0	

[a]The original octahedron in the b.c.c. lattice.

Fig. 8. The ω structure viewed in the original b.c.c. lattice. The position equivalent to that of the N atom in ϵ-TaN is shown by a cross.

$$a_{hex} \approx \sqrt{2} a_{bcc}$$

$$c_{hex} \approx \sqrt{\frac{3}{2}}\, a_{bcc}$$

In ϵ-TaN, however, $a_{hex} \approx 1.57 a_{bcc}$ is a little larger, while $c_{hex} \approx 0.88 a_{bcc}$ approximates to the above correlation.

The large a_{hex} in ϵ-TaN allows the accommodation of the N atoms at $z = 0$. The N atoms are positioned in the distorted octahedral cavities of the metal sublattice, but actually off centre of it. In other words, the N atoms are coordinated by five Ta atoms in a four-sided pyramid; four Ta(2) atoms are at 0.216 nm and one Ta(1) atom at 0.204 nm from the N atom [28]. Hence between pure Ta ($a = 0.330$ nm) and ϵ-TaN there are differences in the distances (nanometres) associated with the octahedral site.

	From the centre to the corners of the octahedron in b.c.c. Ta	→	From the N atom to the Ta atoms in ϵ-TaN
First-nearest neighbours	0.165 (×2)	→	0.216 (×2)
Second-nearest neighbours	0.234 (×4)	→	0.216 (×2), 0.204 (×1)

In Fig. 8 the first-nearest neighbours to the centre of the octahedron (solid circle) of the b.c.c. lattice are the atoms numbered 6 and 9; the second-nearest neighbours are atoms 1, 4, 7 and 8.

There seem to be no experimental data on the position of the N atoms in β-Zr. There are, however, observations on other metals showing the b.c.c lattice response to interstitial nitrogen. Danilkin *et al.* [31] have studied the vibrational spectrum of N atoms in b.c.c.-V ($a = 0.302$ nm). The spectrum obtained for the V–(3–5)at.%N alloy was explained by positioning the N atom in the distorted octahedral site of the b.c.c. lattice, which is further deformed to accommodate this atom. The changes in the distances (nanometres) are similar to those found for ϵ-TaN.

From the centre to the corners of the octahedron	→	From the N atom to the V atoms
0.151 (×2)	→	0.192 (×2)
0.214 (×4)	→	0.201 (×4)

The first-nearest neighbours to N are pushed away by about 30% and the second-nearest neighbours are pulled in by 5%–10%.

Local lattice distortions have also been found in dilute interstitial alloys of Nb with nitrogen and oxygen, in which ω-phase-like diffuse neutron-scattering intensities were observed [32]. In the case of Nb–N alloys the displacements around the N atoms were similar to the above cases: the first neighbours were pushed away by 30% and the second neighbours pulled in by 8.5%.

We do not have direct evidence that b.c.c.-Zr exhibits a similar local lattice distortion around N impurities, but Zr among the b.c.c. metals is very susceptible to the b.c.c. → ω phase transition.

The local lattice distortions discussed above are certainly related to the fact that the b.c.c. transition metals in general exhibit instabilities to lattice strains in the [111] direction [33]. The "ϵ-TaN"-type or the ω-like structure may be an answer to the problem of accommodating the N atoms in the b.c.c. lattice. However, this does not necessarily mean that the origin of this type of local lattice distortion is solely the volume mismatch between the nitrogen atom and the octahedral site of the b.c.c. lattice. Thermodynamically, the volume mismatch effect appears as the positive contribution to ΔG_f from the strain energy, which should be rather small in this case because of the lattice instability in

the [111] direction. However, the raised liquidus–solidus with increasing nitrogen content in b.c.c.-Zr (β-Zr) shows that this strain energy term is more than offset by the enhanced bonding due to the addition of p electrons of nitrogen to the lattice. It is most likely that the ω-like distortions in the interstitial alloys of the b.c.c. metals are electronic rather than mechanical (volume mismatch) in origin.

References

1 L. Kaufman and H. Bernstein, *Computer Calculation of Phase Diagrams*, Academic, New York, 1970.
2 J. Hafner, Quantum theory of structure: sp-bonded systems, in F.R. de Boer and D.G. Pettifor (eds.), *The Structures of Binary Compounds*, North-Holland, Amsterdam, 1989, pp. 147–286.
3 D.G. Pettifor and R. Podloucky, *J. Phys. C: Solid State Phys., 19* (1986) 285–313.
4 D.G. Pettifor and R. Podloucky, *Phys. Rev. Lett., 53* (1984) 1080–1083.
5 L. Brewer, *J. Nucl. Mater., 51* (1974) 2–11.
6 K. Schwarz, *J. Phys. C: Solid State Phys., 10* (1977) 195–210.
7 K. Schwarz, H. Ripplinger and A. Neckel, *Z. Phys. B, 48* (1982) 79–87.
8 O. Kubaschewski-von Goldbeck, *At. Energy Rev., Special Issue No. 6* (1976) 98–99.
9 M. Hillert and L.-I. Staffanson, *Acta Chem. Scand., 24* (1970) 3618–3626.
10 T. Ogawa, *Scr. Metall., 16* (1980) 1309–1313.
11 B. Sundam and J. Agren, *J. Phys. Chem. Solids, 42* (1981) 297–301.
12 M. Hillert, *Calphad, 4* (1980) 1–12.
13 H.A.J. Oonk, *Phase Theory*, Elsevier, Amsterdam, 1981.
14 H.K. Lukas, E.-Th. Henig and B. Zimmermann, *Calphad, 1* (1977) 225–236.
15 T. Ogawa and T. Iwai, *JAERI-M 89-063*, 1989 (Japan Atomic Energy Research Institute).
16 C.B. Alcock, K.T. Jacob, S. Zador, O. Kubaschewski von Goldbeck, H. Nowotny, K. Seifert and O. Kubaschewski, *At. Energy Rev., Special Issue No. 6* (1976) 28–31.
17 G. Eriksson and K. Hack, *Metall. Trans. B, 21* (1990) 1013–1023.
18 M. Hoch, D.P. Dingledy and H.L. Johnston, *J. Am. Chem. Soc., 77* (1955) 304–306.
19 Yu. F. Khromov and D.E. Svistunov, *Izv. Akad. Nauka SSSR, Neorg. Mater., 27* (1991) 25–28.
20 K.A. Gingerich, *J. Chem. Phys., 49* (1968) 14–18.
21 M.A. Eron'yan, R.G. Avarbe and T.A. Nikol'skaya, *Izv. Akad. Nauka SSSR, Neorg. Mater., 12* (1976) 247–249.
22 A. Itoh, M. Akabori, T. Ogawa and M. Ugajin, *1993 Spring Mtg. Atomic Energy Society of Japan*, Paper K-6.
23 T. Ogawa and T. Iwai, *J. Less-Common Met., 170* (1991) 101–108.
24 T. Ogawa and M. Akabori, *Actinides-93, Santa Fe, NM, 1993.*
25 A.N. Christensen and S. Fregerslev, *Acta Chem. Scand., 31* (1977) 861–868.
26 L.E. Toth, *Transition Metal Carbides and Nitrides*, Academic, New York, 1971.
27 L.M. Howe, *Nucl. Instrum. Methods, Phys. Res. Sci. B, 64* (1992) 246–250.
28 A.N. Christensen and B. Lebech, *Acta Crystallogr. B, 34* (1978) 261–263.
29 V.F. Petrunin and N.I. Sorokin, *Izv. Akad. Nauka SSSR, Neorg. Meter., 18* (1982) 2005–2008.
30 B.A. Hatt and J.A. Roberts, *Acta Metall., 8* (1960) 575–584.
31 S.A. Danilkin, V.P. Minaev, V.V. Sumin and A.I. Choklo, *Sov. Phys. – Solid State, 33* (1991) 1–3.
32 H. Dosh, A. van Schwerin and J. Peisl, *Phys. Rev. B, 34* (1986) 1654–1661.
33 Ch. Herzig, Anomalous fast diffusion in metals, in F.J. Kedves and D.L. Beke (eds.), *DIMETA-82 Diffusion in Metals and Alloys*, Trans Tech, Rockport, MA, 1983, pp. 23–38.